Comparison of parallel-plate and in-plane poled polymer films for terahertz sensing

Colin V. McLaughlin, Xuemei Zheng, and L. Michael Hayden*

Department of Physics, University of Maryland, Baltimore County, Baltimore, Maryland 21250, USA

*Corresponding author: hayden@umbc.edu

We have performed calculations and measurements of the efficacy of two poling geometries of poled electro-optic (EO) polymer films for use in sensing terahertz (THz) radiation via EO sampling. Taking reflective and absorptive losses into consideration, we find that a parallel-plate (PP) poled film has a sensitivity maximum when oriented at 55° to the incident probe and THz beams. In addition, we show that our in-plane (IP) poled polymer films are comparable in sensitivity to PP-poled films and discuss the potential for improving IP-poled polymer devices.   © 2007 Optical Society of America

OCIS codes: 160.2100, 160.4890, 190.4360, 190.4400, 190.7110, 250.2080.

1. Introduction

Poled electro-optic (EO) polymers have recently been shown to emit and detect broadband terahertz (THz) radiation [1]. Effective THz sensors operating in the wavelength vicinity of 3 mm to 30 μm are important in applications ranging from semiconductor materials characterization to biomedical imaging [2]. EO crystals [3], photoconducting dipole antennae [4,5], and poled EO polymer films [1,6,7] have been used as THz sensors. Sensors utilizing EO polymers are desirable because of their broadband, gap-free response [1,6,8]. To our knowledge, a full analysis of poled polymer devices for THz sensing has not been previously presented. In this paper we provide such an analysis for two different poling geometries, parallel-plate (PP) and in-plane (IP). We theoretically and experimentally explore angle tuning of PP-poled EO polymer sensors to optimize the detected THz signal. Modeling of the electric field distribution in the IP-poling geometry is conducted for evaluating the poling efficiency and for use in evaluating the EO measurement. Finally, the detected THz signals from the IP- and PP-poled polymers are compared.

Typical EO polymer poling methods employ a PP design, where a thin polymer layer is sandwiched between two electrodes. The electrodes usually consist of either indium tin oxide (ITO) and evaporated gold or ITO–ITO. To use the PP-poled polymer as a THz sensor, the high reflectivity of metal in the THz regime requires that the one or both of the electrodes be removed. The resulting poled, free-standing film makes subsequent poling of that sample difficult or impossible. In contrast, IP-poled EO polymer devices permit the probe and THz beams to pass through the polymer without obstruction from the electrodes, allowing for subsequent or *in situ* poling. Recent studies show that EO glasses can exhibit considerably higher EO coefficients (>250 pm/V) than the poled polymers presented here (~30 pm/V) [9]. However, because of their fragility, these EO glasses are not currently well suited for PP poling in a thick-film (~100 μm) form. IP poling, which requires fewer processing steps than PP poling, can be used with these EO glasses. It should also be stressed that IP poling allows for optimal overlap of the THz electric field with the poling direction (z axis) of the oriented chromophores in the poled film, increasing the detected signal in THz sensing. An IP-poled polymer sensor is oriented such that the incident THz beam is normal to the polymer surface, fully aligning the polymer z axis with the THz polarization. As will be shown, this optimal alignment leads to more efficient THz sensing. In contrast, utilizing a PP-poled EO polymer sensor requires rotation of the polymer film with respect to the

incident THz beam to allow an appreciable component of the THz electric field to be aligned with the film's poled z axis.

2. Theory

The sensitivity of an EO sampling sensor is directly proportional to the phase retardation induced by the external THz electric field. To compare IP poling to PP poling for use in THz sensing, the THz-induced retardation [10], due to the EO effect, between the s and p polarization of the optical probe beam needs to be determined for both cases. For both the IP- and PP-poled sensors we utilize a half-wave plate to rotate the probe beam polarization such that the s and p components are of equal amplitude [Figs. 1(a) and 1(b)]. The PP-poled sensor is aligned such that the THz beam, which is collinear with the optical probe, is purely p-polarized, with a projection along the z axis (poling axis) of the polymer [Fig. 1(b)]. For the PP-poling case, the change in the optical path difference of the p-polarized (l_p) and s-polarized (l_s) component of the optical probe beam within the polymer is given by

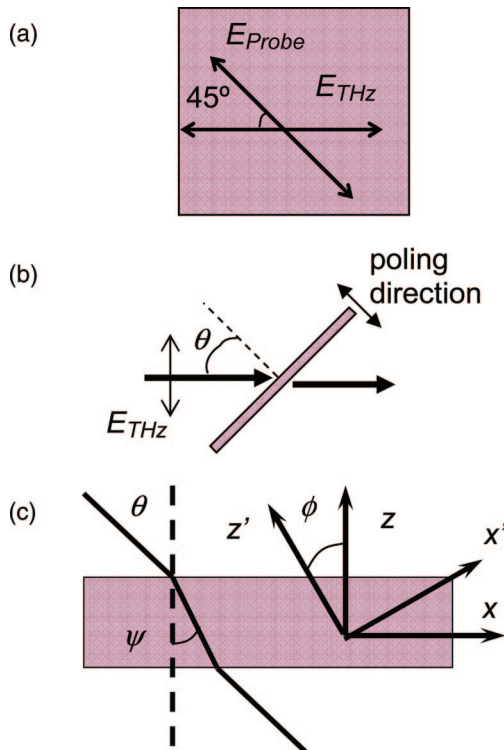$$\Delta(l_p - l_s) = \frac{d_{PP}}{\cos \psi}(\Delta n_p - \Delta n_s), \qquad (1)$$

(a)

E_{Probe}

45°

E_{THz}

(b)

poling direction

θ

E_{THz}

(c)

θ

z' ϕ z

x'

x

ψ

Fig. 1. (Color online) Schematic of the PP-poled polymer THz sensor. (a) The probe beam is polarized at 45° to the THz beam and (b) both are incident at an angle, θ, and (c) copropagate through the polymer at an angle, ψ. The poling direction is the z axis. The principle axes are rotated by ϕ about the y axis in the presence of the THz electric field.

where d_{PP} is the PP polymer thickness and ψ is the refracted angle. The modulated indices for the s and p polarization are, respectively, Δn_s and Δn_p. To derive Eq. (1), we have used the fact that without the presence of the THz electric field the static refractive index and refracted angle of the s and p components are approximately equal [$(n_s \approx n_p \approx n)$, $(\psi_s \approx \psi_p \approx \psi)$] within the polymer. The probe beam is incident upon the polymer at an angle θ, leading to $\sin \psi = (1/n)\sin \theta$ [Fig. 1(c)]. The applied THz electric field is

$$E_x^{THz} = E^{THz} \cos \psi^{THz},$$

$$E_y^{THz} = 0,$$

$$E_z^{THz} = E^{THz} \sin \psi^{THz}, \qquad (2)$$

where ψ^{THz} is the refracted angle of the THz beam within the polymer. The poled polymer has a symmetry of ∞ mm, which has an EO coefficient tensor of the form [11]

$$r_{Ik} = \begin{pmatrix} 0 & 0 & r_{13} \\ 0 & 0 & r_{13} \\ 0 & 0 & r_{33} \\ 0 & r_{51} & 0 \\ r_{51} & 0 & 0 \\ 0 & 0 & 0 \end{pmatrix}. \qquad (3)$$

The resulting associated index ellipsoid for the poled polymer affected by the presence of the THz field is

$$\left(\frac{1}{n_o^2} + r_{13}E_z^{THz}\right)x^2 + \left(\frac{1}{n_o^2} + r_{13}E_z^{THz}\right)y^2$$
$$+ \left(\frac{1}{n_e^2} + r_{33}E_z^{THz}\right)z^2 + \left(2r_{51}E_x^{THz}\right)xz = 1. \qquad (4)$$

To remove the cross term associated with xz, we perform a coordinate system transformation into x', y', and z' in which the principle x and z axes are rotated through an angle ϕ [Fig. 1(c)], such that

$$x = x' \cos \phi - z' \sin \phi,$$

$$y = y',$$

$$z = x' \sin \phi + z' \cos \phi. \qquad (5)$$

Elimination of the cross term ($x'z'$) in the new coordinate system requires that

$$\tan 2\phi = \frac{2r_{51}E_x^{THz}}{(1/n_o^2 + r_{13}E_z^{THz}) - (1/n_e^2 + r_{33}E_z^{THz})}. \qquad (6)$$

It is characteristic of poled polymers that the ratio of r_{13} and r_{51} to r_{33} is approximately one-third [11]. Tak-

ing $n_o \approx n_e \approx n$ and combining Eq. (2) and Eq. (6), we arrive at

$$\tan 2\phi = -\frac{E_x^{THz}}{E_z^{THz}} = \frac{-\cos \psi^{THz}}{\sin \psi^{THz}}. \qquad (7)$$

In the new coordinate system we obtain

$$\frac{1}{n_{x'}^2} = \frac{1}{n^2} + \frac{r_{33}E_z^{THz}}{3} + \frac{2r_{33}E_z^{THz}\sin^2\phi}{3}$$
$$+ \frac{2r_{33}E_x^{THz}\sin\phi\cos\phi}{3},$$

$$\frac{1}{n_{y'}^2} = \frac{1}{n^2} + \frac{r_{33}E_z^{THz}}{3},$$

$$\frac{1}{n_{z'}^2} = \frac{1}{n^2} + \frac{r_{33}E_z^{THz}}{3} + \frac{2r_{33}E_z^{THz}\cos^2\phi}{3}$$
$$- \frac{2r_{33}E_x^{THz}\sin\phi\cos\phi}{3}. \qquad (8)$$

From Eq. (8), we can derive indices along the new principle x', y', and z' axes. Taking $(1/3)n^2r_{33}E_z \ll 1$, the induced modulated index in the s-polarized state is given by $\Delta n_s = \Delta n_{y'} = (1/6)n^3r_{33}E_z$. The index for the p-polarized state is

$$\frac{1}{(n_p)^2} = \frac{\sin^2(\phi - \psi)}{n_{z'}^2} + \frac{\cos^2(\phi - \psi)}{n_{x'}^2}, \qquad (9)$$

where propagation relative to the z' axis is given by the angle $(\phi - \psi)$. The resulting modulated index in the p-polarized state is given by

$$\Delta n_p = \frac{n^3r_{33}}{6}\{[1 + 2\sin^2\psi + \sin 2\phi \sin(2\phi - 2\psi)]E_z$$
$$+ \sin 2\phi \cos(2\phi - 2\psi)E_x\}. \qquad (10)$$

Using the fact that the THz index ($n_{THz} = 1.7$) is nearly constant from 1–8 THz and approximately equal to the optical index at 800 nm [8], we have $\sin \psi^{THz} \approx \sin \psi \approx (1/n)\sin \theta$ and Eq. (1) can be simplified using Δn_s and Δn_p to give

$$\Delta(l_p - l_s) = \frac{d_{PP}n^3r_{33}}{3}E^{THz}\frac{\sin \theta}{\sqrt{n^2 - \sin^2 \theta}}. \qquad (11)$$

This result shows that the maximum THz-induced retardation occurs when the poling direction (polymer z axis) is parallel to the THz polarization and the incident angle is 90° [Fig. 2(a)]. However, this does not account for reflective losses of the THz and optical beams at the surfaces of the polymer. Including an angle-dependent Fresnel transmission factor, $F_{THz}(\theta)$,
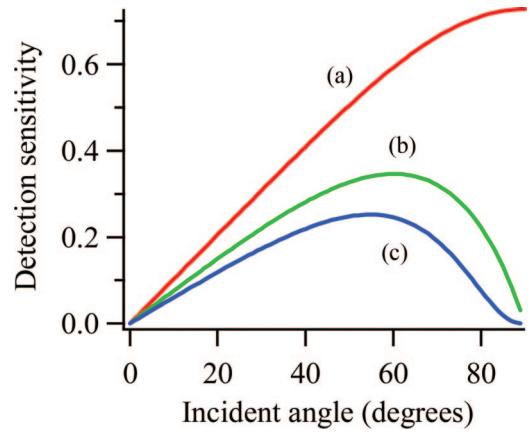

Fig. 2. (Color online) (a) Detection sensitivity due to THz-induced retardation for the PP-poled EO polymer THz sensor as a function of sensor incident angle, θ. (b) Inclusion of THz loss due to Fresnel reflection produces a maximum sensitivity at an incident angle of 60°. (c) Accounting for optical probe absorption in the polymer and reflective losses at the air–polymer and polymer–air boundaries further attenuates the sensitivity and brings the optimal sensing angle to 55°.

for the THz field due to reflective loss at the air–polymer front interface and ignoring THz absorption inside the polymer, the detected signal $S(\theta)$ is represented by

$$S(\theta) \propto \Delta(l_p - l_s)F_{THz}(\theta), \qquad (12)$$

where

$$F_{THz}(\theta) = \frac{2n_{air}\cos \theta}{n_{air}\cos \psi^{THz} + n_{THz}\cos \theta}. \qquad (13)$$

The THz transmission factor causes an amplitude reduction throughout the angle tuning range [Fig. 2(b)] and the detected signal maximum is shifted to an angle of $\theta \approx 60°$. The detected signal will be further modified by probe beam loss at both the front and rear surface of the polymer. Similarly, absorption of the probe beam within the polymer will also affect the detected signal amplitude. The inclusion of another factor, $F_{Opt}(\theta)$, to account for these losses is therefore required and is given as follows:

$$F_{Opt}(\theta) = T(\theta)\exp\left(\frac{-nd_{PP}\alpha}{\sqrt{n^2 - \sin^2 \theta}}\right), \qquad (14)$$

where the transmission intensity term, $T(\theta)$, accounts for the total transmission of the probe beam through the polymer. The exponential is the absorptive loss term corresponding to the actual polymer thickness transected by the optical beam, where α is the absorption coefficient. The transmission intensity term, $T(\theta)$, is calculated by separating the s- and p-polarized components of the optical beam and independently calculating their respective transmission amplitudes. The two attenuated com-

ponents are then combined to form the probe beam transmission intensity:

$$T(\theta) = \frac{1}{2} \left\{ \left[\frac{4n^2 \cos\theta \sqrt{n^2 - \sin^2\theta}}{\left(n^2 \cos\theta + \sqrt{n^2 - \sin^2\theta}\right)^2} \right]^2 + \left[\frac{4\cos\theta \sqrt{n^2 - \sin^2\theta}}{\left(\cos\theta + \sqrt{n^2 - \sin^2\theta}\right)^2} \right]^2 \right\}. \quad (15)$$

Including probe beam losses and the THz transmission factor, the detected signal for a PP-poled sample is

$$S_{PP}(\theta) \propto \Delta(l_p - l_s) F_{THz}(\theta) F_{Opt}(\theta). \quad (16)$$

The optimum angle for THz sensing using a PP-poled EO polymer, accounting fully for optical and THz reflection and optical absorption, is ~55° [Fig. 2(c)].

As discussed above, because of the poling geometry, EO sensing with a PP-poled polymer requires that the film be rotated, permitting only a partial projection of the THz field to be detected. In contrast, IP poling aligns the z axis of the polymer perpendicular to the polymer surface normal. This allows for a full projection of the THz electric field onto the poling direction in the case of normal incidence of the THz beam. The THz-induced retardation between the two polarization components of the optical probe beam in an IP-poled configuration can be shown to be

$$\Delta_{IP}(l_P - l_S) = \frac{d_{IP} n^3 r_{33} E^{THz}}{3}, \quad (17)$$

where d_{IP} is the IP polymer thickness. As in the case of PP poling, we need to consider THz amplitude reduction and probe beam reflective loss at the air–polymer interface. Because the poled polymer is not removed from the IP-poling device, probe beam reflective loss at polymer–fused-silica-substrate and fused-silica-substrate–air boundaries must also be considered. These factors are combined in a total attenuation factor given by

$$F_{IP} = \frac{2}{n_{THz} + 1} \left[\frac{4n}{(n+1)^2} \right] \left[\frac{4n n_{fs}}{(n + n_{fs})^2} \right] \left[\frac{4n_{fs}}{(1 + n_{fs})^2} \right]. \quad (18)$$

The THz and optical polymer index of $n_{THz} \approx n \approx 1.7$ [8] and optical fused-silica index of $n_{fs} = 1.453$ (at 800 nm) result in an amplitude attenuation and reflective loss factor of $F_{IP} = 0.663$. Including probe beam absorption in the polymer, we arrive at a general expression for the detected signal in an IP-poled sensor of

$$S_{IP} \propto F_{IP} \Delta_{IP}(l_P - l_S) \exp(-d_{IP}\alpha). \quad (19)$$

The ratio of the detected IP-poled signal (S_{IP}) to the maximum detected PP-poled signal at the optimum angle [$S_{PP}(\theta = 55°)$], assuming equal polymer thicknesses and EO coefficients, is 2.4.

3. Experiment

Our polymer sensor films are guest–host mixtures of 40 wt. % of the dye (3-(2-(4-(N,N-diethylamino)-phenyl)ethenyl)-5,5-dimethyl-1,2-cyclohexenylidene)-propanedinitrile (Lemke) and 60 wt. % amorphous polycarbonate (APC). The dye molecule was obtained from Battelle Corporation (Columbus, Ohio, USA) and the polymer from Aldrich Chemical (St. Louis, Missouri, USA). The polymer films are made by casting a solution of the dye molecule and host polymer in dicholoroethane (12%/88% solid-to-solvent mass ratio) onto the substrates through a 0.2 μm filter. Solvent removal is accomplished through a soft bake at 80 °C for 4 h under normal atmospheric conditions, followed by a hard bake at 105 °C for 12 h in vacuum.

The IP-poling devices consist of 3 μm aluminum electrodes on a substrate of 1 mm thick fused silica. The electrodes are separated by a gap of 100 μm and have a parallel face of 1 cm in length [Figs. 3(a) and 3(b)]. It should be noted that rounded electrode edges reduce the high-field fringing effects that are present with sharp edges, thereby reducing the occurrence of polymer dielectric breakdown during poling. The IP device requires only drop casting of the polymer solution, with the film thickness controlled by the mass-to-solvent ratio and solution volume applied. The PP device is created by casting the polymer solution onto an ITO-coated substrate. After solvent removal, we press several polymer films between two ITO substrates, at approximately 80° above the glass-transition temperature (T_g), using 75 μm thick polyimide spacers between the substrates to create a uniformly thick film. A nonzero EO coefficient is imparted to both the IP and PP films through standard electric field poling [12]. The maximum poling tem-
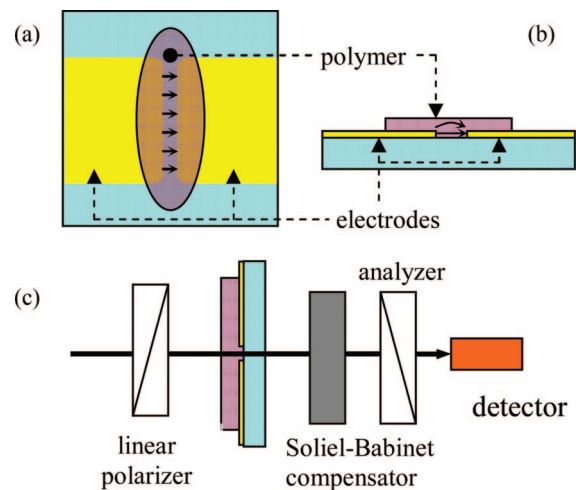
Fig. 3. (Color online) (a) Top and (b) side views of the IP-poling device. The poling electrodes are 3 μm thick and are separated by a 100 μm gap. The arrows within the electrode gap in (a) and (b) denote the poling field. (c) Measurement of the EO coefficient in an IP sample utilizes a modified transmission-geometry setup.

perature for Lemke/APC (LAPC) (40%/60%) is 90 °C, which is 5 °C below T_g.

The EO coefficients of the PP- and IP-poled polymers are measured using a transmission-geometry setup [13]. In both cases, modulation of the incident beam (I_{mod}) is a result of polarization rotation due to the EO effect induced by an externally applied electric field of frequency Ω and has the form

$$I_{mod} = \left(\frac{I_{max} - I_{min}}{2}\right)\Delta\Gamma \sin(\Omega t). \qquad (20)$$

The maximum EO phase shift is given by $\Delta\Gamma$. The terms I_{max} and I_{min} are determined through rotation of the Soliel–Babinet compensator and are, respectively, the maximum and minimum intensity at the detector. We let the amplitude of the modulated signal be defined as

$$A = \left(\frac{I_{max} - I_{min}}{2}\right)\Delta\Gamma, \qquad (21)$$

where the EO phase shift is given by

$$\Delta\Gamma = \frac{2\pi d}{\lambda}\left(\frac{\delta n_p}{\cos \psi_p} - \frac{\delta n_s}{\cos \psi_s}\right), \qquad (22)$$

for a polymer of thickness d. The wavelength is λ and δn_p and δn_s are the modulated indices in the p and s polarizations, respectively. A polarizer placed before the sample provides linearly polarized light at 45° to the polymer z axis. The PP-poled sample requires rotation with respect to the incident beam, as in Fig. 1(b) [13]. However, because of the poling geometry, the IP setup utilizes normal incidence, leading to $\psi_{s,p} = 0$ [Fig. 3(c)]. For clarity, we define $n_p = n_e$ and $n_s = n_o$, where n_e is the index in the polymer z axis. The resulting phase shift for the IP case is

$$\Delta\Gamma = \frac{2\pi d_{IP}}{\lambda}(\delta n_e - \delta n_s). \qquad (23)$$

Recalling that $r_{13} \approx (1/3)r_{33}$ [11], the modulated indices are, respectively,

$$\delta n_e = \frac{1}{2} n^3 r_{33} E_z,$$

$$\delta n_o = \frac{1}{6} n^3 r_{33} E_z, \qquad (24)$$

where n is the optical index of the polymer. Unlike a PP-poling configuration where the applied electric field (E_z) is highly uniform and is expressed as the applied voltage divided by the polymer thickness, in an IP-poling configuration E_z is highly nonuniform due to fringing effects. Therefore, we modeled the electric field distribution of our IP device using a commercially available finite-element analysis package [14]. The results of these simulations (Fig. 4) are
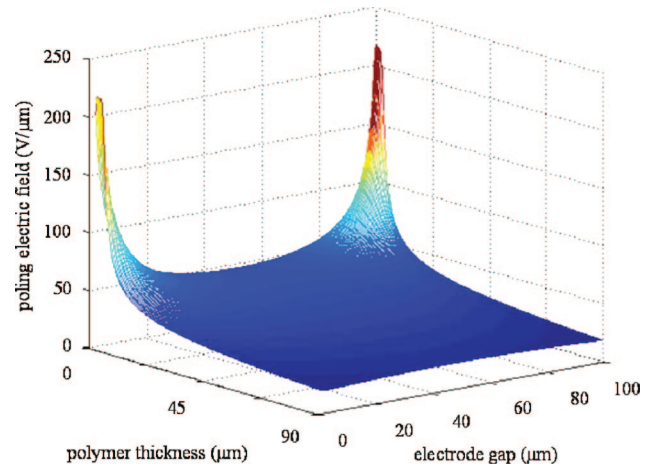

Fig. 4. (Color online) Simulation of the poling field through a 90 μm thick polymer in an IP device. This is a model of 7 kV applied to 3 μm thick electrodes with a 100 μm wide gap on a fused-silica substrate. The extremely high fields surrounding the electrodes limit the poling efficiency through the rest of the polymer. The average field (E_{eff}) in this simulation is 36.5 V/μm.

in excellent agreement with previous studies [15] and show that the average E_z in the polymer (across and above the electrode gap) is proportional to the applied voltage and is a function of the polymer thickness. For a first approximation, we assume uniform illumination of the electrode gap by the incident laser beam and replace E_z in Eq. (24) with the average electric field within the polymer, E_{eff}. Using Eq. (24) with Eqs. (21) and (23) and solving for r_{33}, we arrive at a detected EO coefficient for an IP-poled polymer of

$$r_{33} = \frac{3\lambda}{\pi d_{IP} n^3} \frac{1}{(I_{max} - I_{min})}\left(\frac{A}{E_{eff}}\right). \qquad (25)$$

Because of the E_{eff} factor, the reported EO coefficients for our IP-poled polymers are an averaged value for the full width and thickness of the polymer in the electrode gap.

We used both types of poled polymer geometry as EO sensors in a standard THz setup (Fig. 5). A 1 kHz,
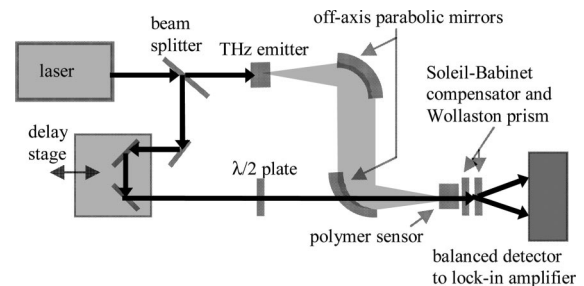

Fig. 5. Schematic of the THz setup. A pellicle beam splitter splits the probe and pump beams. The pump generates THz in an EO crystal or poled polymer film. The half-wave plate is used to rotate the probe beam polarization 45° with respect to the THz polarization. Both the THz and probe are focused onto the polymer sensor and a balanced detection scheme records the THz electric field.

800 nm centered, 45 fs FWHM pulse train from a Ti:sapphire laser is split by a pellicle into a probe and pump beam, after which the pump beam is used to generate THz in either a poled polymer or EO crystal. Off-axis parabolic mirrors collimate and focus the THz beam onto the poled polymer sensor. Collinearly propagating with the THz beam, the probe beam is also focused into the poled polymer sensor. When using a PP-poled sensor, the polymer is placed such that the incident THz beam electric field is p-polarized at an incident angle, θ, with respect to the polymer [Fig. 1(c)]. An IP-poled polymer sensor is oriented so that the probe and THz beams are incident normal to the polymer surface. For both cases, the optical probe beam is polarized at 45° with respect to the THz polarization. EO modulation of the probe beam by the THz electric field is then recorded through a balanced detection scheme. Fourier transformation of the detected THz electric field yields the THz amplitude spectrum.

4. Results and Discussion

We obtained lower values of the EO coefficient (r_{33}) in an IP-poled polymer film than that obtained in a PP-poled sample with an equivalent applied voltage and electrode separation. This is consistent with our modeling and is expected due to the fringing effects of the thin electrodes of the IP device resulting in a nonuniform electric field, as discussed above. The analytically derived electric field at the center of the electrode gap for an IP geometry with an infinitely thin electrode is reported to be $E_{center} = (2/\pi)*(V/g)$ [15], where V is the applied voltage and g is the electrode gap. Our simulation accurately recovers this value at the midpoint of the gap but rises sharply near the electrode edges as expected. We calculate E_{eff} by averaging the value of the electric field at each grid point between the electrodes up to the thickness of the polymer.

Modeling of our IP device yields an average effective electric field in the z direction of $E_{eff} = 36.5$ V/μm for a 90 μm thick polymer, a 100 μm electrode gap, 3 μm thick electrodes on fused silica, and an applied voltage of 7 kV (Fig. 4). An IP-poled film corresponding to the above specifications had a measured EO coefficient of $r_{33} = 12.4$ pm/V. Previously, we studied the relationship between the poling field and the measured r_{33} in PP-poled LAPC [16]. Using these results, we predict that LAPC poled at 36 V/μm should have an EO coefficient of $r_{33} \approx 12$ pm/V.

After EO measurements, we conducted THz experiments with both sensors. To compare the angle-dependent sensitivity of a PP-poled sample with our theory, angle tuning of an 82 μm thick PP sensor ($r_{33} = 29.7$ pm/V) was conducted using the THz setup previously described. The THz emitter for this study was a PP-poled polymer film. THz electric field traces were taken at various sensor angles, θ, between 20° and 85°. Four traces were recorded at each angle and then averaged. The averaged electric field traces were Fourier transformed to allow comparison of am-

plitudes at specific frequencies. Figure 6 shows the THz amplitude as a function of sensor angle at the frequencies of 1 and 1.5 THz. Equation (16) was used to fit the data by adjusting only the overall amplitude. The incident angle, θ, was measured in the THz setup, and experimentally determined values for α, n, $r_{33}(PP)$, and d_{PP} were held as constants in the fit. There is good agreement between the frequency amplitude measurements and their associated fits.

We also compared the IP- and PP-poling geometry for EO THz sensing. A 1 mm thick ZnTe (110) crystal was used as the THz emitter. The PP-poled film had a measured thickness of 75 μm and an EO coefficient of $r_{33} = 27.5$ pm/V and was placed as a THz sensor at an angle of $\theta = 60°$. The IP-poled polymer film was 90 μm thick with an average effective EO coefficient of $r_{33} = 12.4$ pm/V. According to our theory [Eqs. (16) and (19)], the sensing ratio for the two sensors described above should be $S_{IP}/S_{PP}(\theta = 60°) = 1.3$. Experimentally, we are able to measure the ratio between 0.4 and 2.4 THz, as limited by the ZnTe emitter. The measured ratios over the detectable range fall within 15% of the predicted ratio of 1.3 (Fig. 7). The THz time domain traces (Fig. 7, lower inset) have a similar shape for both sensors, indicating that the IP electrodes do not lead to a time integration of the incident THz field [7].

Improvement upon the IP device is possible through several methods. According to our simulations, thicker IP electrodes will lead to a more uniform electric field, translating to more efficient poling of the EO polymer, a higher EO coefficient (r_{33}), and better THz sensing. For a 90 μm thick polymer, our model shows that electrodes 30 μm thick would provide a 40% higher average poling field than the current 3 μm thick electrodes, thereby increasing the THz sensing efficiency by 40%. Also, our current THz experiment does not allow tight focusing of the probe beam. As a result, 70% of the probe beam intensity is
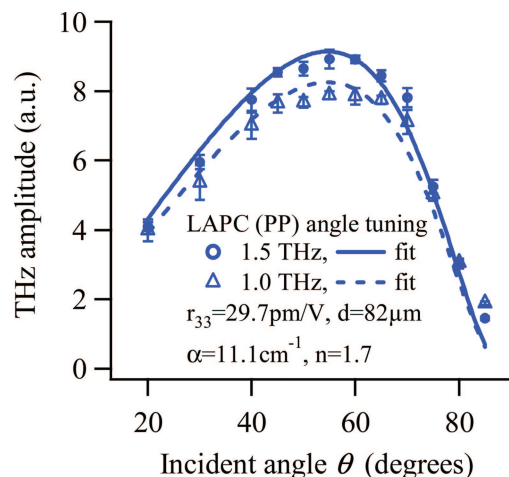

Fig. 6. (Color online) The amplitude fits above use the full expression for angle-dependent THz sensing of a PP-poled EO polymer [Eq. (16)]. The two frequencies reported were simultaneously retrieved from Fourier-transformed THz electric field traces.
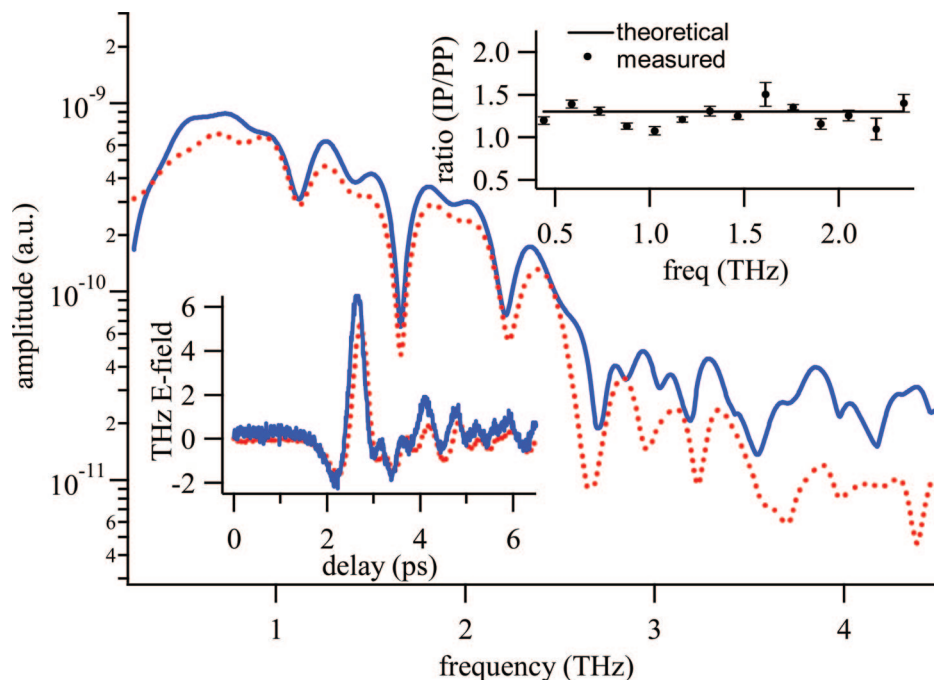
Fig. 7. (Color online) THz amplitude spectrum from IP (solid curves) and PP (dotted curves) polymer sensors. The PP-poled sensor was placed at an angle of θ = 60°. Upper inset, comparison of the measured and theoretical ratio (S_{IP}/S_{PP}) of the THz amplitudes for the two sensor geometries. Lower inset, THz electric field traces for the two EO polymer sensor poling geometries.

blocked by the small (100 μm) gap of the IP electrodes, resulting in a low probe beam intensity at the detectors and a decrease in the signal-to-noise ratio for the IP device. Therefore, it is reasonable to assume that a 70% increase in the detected signal is possible through tighter probe beam focusing.

5. Conclusion

In conclusion, we have studied the application of EO polymers for THz sensing. Two geometries of polymer poling, IP and PP, are studied and compared with regard to their sensitivity as EO sensors. Measurements and calculations show the optimum sensing angle for a PP-poled EO polymer sensor to be ∼55° with respect to the incident probe and THz beams. Our modeling of the electric field distribution for an IP-poled polymer concurs with previous studies and the measured EO values using this model are consistent with previously developed poling and measurement methods for polymers poled in a sandwich geometry between two electrodes (PP). The model also provides a base for design improvements of the IP device. The current IP-poled polymer film shows comparable THz sensing properties to the PP-poled film and has potential for improvement.

References

1. X. Zheng, A. Sinyukov, and L. M. Hayden, "Broadband and gap-free response of a terahertz system based on a poled polymer emitter-sensor pair," Appl. Phys. Lett. **87,** 081115 (2005).
2. X. C. Zhang, "Materials for terahertz science and technology," Nature Materials **1,** 26–33 (2002).
3. A. Schneider, M. Neis, M. Stillhart, B. Rutz, R. U. A. Khan, and P. Gunter, "Generation of terahertz pulses through optical rectification in organic DAST crystals: theory and experiment," J. Opt. Soc. Am. B **23,** 1822–1835 (2006).
4. M. van Exter, C. Fattinger, and D. Grischkowsky, "Terahertz time-domain spectroscopy of water vapor," Opt. Lett. **14,** 1128–1130 (1989).
5. Y. C. Shen, P. C. Upadhya, H. E. Beere, E. H. Linfield, A. G. Davies, I. S. Gregory, C. Baker, W. R. Tribe, and M. J. Evans, "Generation and detection of ultrabroadband terahertz radiation using photoconductive emitters and receivers," Appl. Phys. Lett. **85,** 164–166 (2004).
6. H. Cao, T. F. Heinz, and A. Nahata, "Electro-optic detection of femtosecond electromagnetic pulses by use of poled polymers," Opt. Lett. **27,** 775–777 (2002).
7. A. Nahata, D. H. Auston, T. F. Heinz, and C. Wu, "Coherent detection of freely propagating terahertz radiation by electro-optic sampling," Appl. Phys. Lett. **68,** 150–152 (1996).
8. X. Zheng, C. V. McLaughlin, M. R. Leahy-Hoppa, A. M. Sinyukov, and L. M. Hayden, "Modeling a broadband terahertz system based on an electro-optic polymer emitter sensor pair," J. Opt. Soc. Am. B **23,** 1338–1347 (2006).
9. T.-D. Kim, J. Luo, J.-W. Ka, S. Hau, Y. Tian, Z. Shi, N. M. Tucker, S.-H. Jang, J.-W. Kang, and A. K.-Y. Jen, "Ultralarge and thermally stable electro-optic activities from Diels-Alder crosslinkable polymers containing binary chromophore systems," Adv. Mater. **18,** 3038–3042 (2006).
10. N. C. J. van der Valk, T. Wenckenbach, and P. C. M. Planken, "Full mathematical description of electro-optic detection in

optically isotropic crystals," J. Opt. Soc. Am. B **21,** 622–631 (2004).

11. P. N. Prasad and D. J. Williams, *Introduction to Nonlinear Optical Effects in Molecules and Polymers* (Wiley, 1991).

12. K. D. Singer, J. E. Sohn, and S. J. Lalama, "Second harmonic generation in poled polymer films," Appl. Phys. Lett. **49,** 248–250 (1986).

13. A. Sandalphon, B. Kippelen, K. Meerholz, and N. Peyghambarian, "Ellipsometric measurements of poling birefringence, the Pockels effect, and the Kerr effect in high-performance photorefractive polymer composites," Appl. Opt. **35,** 2346–2354 (1996).

14. FEMLAB 2006, COMSOL AB, Stockholm, Sweden, http://www.comsol.com.

15. M. Stahelin, C. A. Walsh, D. M. Burland, R. D. Miller, R. J. Twieg, and W. Volksen, "Orientational decay in poled second-order nonlinear optical guest-host polymers: temperature dependence and the effects of poling geometry," J. Appl. Phys. **73,** 8471–8479 (1993).

16. L. M. Hayden, A. M. Sinyukov, M. R. Leahy, J. French, P. Lindahl, W. N. Herman, R. J. Twieg, and M. He, "New materials for optical rectification and electrooptic sampling of ultrashort pulses in the terahertz regime," J. Polym. Sci. Part B Polym. Phys. **41,** 2492–2500 (2001).